DFT investigation of pyramidal Au_9M^{2+} and $Au_{19}M$ (M = Sc-Ni): similarities and differences of structural evolution, electronic and magnetic properties

Ngo Thi Lan[1,2,3], **Nguyen Thi Mai**[1,2], **Nguyen Van Dang**[3] **and Nguyen Thanh Tung**[1,2†]

[1]*Institute of Materials Science, Vietnam Academy of Science and Technology,*
18 Hoang Quoc Viet, Cau Giay, Hanoi, Vietnam

[2]*Graduate University of Science and Technology, Vietnam Academy of Science and Technology,*
18 Hoang Quoc Viet, Cau Giay, Hanoi, Vietnam

[3]*Institute of Science and Technology, TNU - University of Science,*
Tan Thinh Ward, Thai Nguyen City Thai Nguyen 250000 Vietnam

E-mail: [†]tungnt@ims.vast.ac.vn

Abstract. *Au_{10}^{2+} and Au_{20} pyramids, whose stability and inertness are comparable to carbon fullerene C60, are considered as important landmarks in the long-history investigation of gold nanoclusters. Numerous experimental and theoretical studies on doping Au_{10}^{2+} and Au_{20} with transition metal atoms have been carried out for specific properties that can be used as advanced material in nanotechnology applications. In this work, we discussed the similarities and differences between the structural, stability, and electronic properties of Au_9M^{2+} and $Au_{19}M$ (M = Sc-Ni) clusters using density functional theory. It is found that except for the preferred dopant site, the structural evolution of Au_9M^{2+} cluster resembles that of $Au_{19}M$ in general. Although the V dopant seems to be the important ingredient for the structural transformation in both species, it is remarkable that the transformation appears stronger in $Au_{19}V$ compared with Au_9V^{2+}. The calculated average binding energies are utilized to identify their relative stable patterns. Depending on the 3d transition metal atom dopant, the spin magnetic moments of Au_9M^{2+} and $Au_{19}M$ clusters vary from 0 to 5 μB, reaching the highest value with the Cr doped species. We show that both Au_9Cr^{2+} and $Au_{19}Cr$ have similarities in the electronic structures and are potential magnetic superatoms.*

Keywords: $Au_{19}Cr$; Au_9Cr^{2+} clusters; density functional theory; superatoms.

Classification numbers: 31.15.E.

1. Introduction

In the past decades, along with the rapid development of nanoscience and nanotechnology, there has been a lot of research focusing on nanoclusters of gold atoms [1–4]. Due to the large fraction of surface atoms and because of quantum size effects, the fascinating picture of gold clusters can be changed suddenly by just adding or removing one atom. For example, small Aun clusters up to n = 8-13 depending on charge states favor planar geometries [5–7] while larger species grow up via hollow cage structures at $n = 14 - 18$ [8, 9], tube-like structure at $n = 24 - 26$ [10, 11], fullerene type at $n = 32$ [12], and the most interesting tetrahedral Au_{20} - an outstanding landmark in cluster science [8]. Exceptionally enhanced stabilities have been observed for the gold clusters whose number of atoms corresponds to the following "magic" values: 2, 8, 18, 20, 34, 58, and 92 owing to their closed electronic supershells [13]. While being inert as bulk material, gold clusters Au_n ($n \leq 20$) exhibit a remarkable odd-even staggering catalytic behavior with Au8 found to be the smallest catalytically active size [14, 15]. In addition, when these tiny clusters are used in reality, it is expected that their unique properties are strongly interfered with appearing additional complexities, for instance, the interactions of carrying substrates or surrounding ambiences. Hence, understanding the geometric and electronic properties of isolated gold clusters, in absence of substrate or ambient interactions, is also a crucial step towards their practical applications. In this regard, the evolutionary laws of geometrical structure, electronic configuration, and stability of gold clusters at different sizes and charge states have been intensively studied through theoretical/computational and experimental methods. Previous search showed that the structural transformation from 2D to 3D occurs at a size $n = 8$ for pure gold clusters in neutral and cationic states [16]. In contrast, this process occurs at a larger size $n = 12$ in the case of anionic species [17, 18]. The neutral gold cluster of 10 atoms is stable in the planar form while the dicationic Au_{10}^{2+} is significantly stabilized in form of a tetrahedral structure [19, 20]. Another remarkably stable stoichiometry is Au_{20} that also prefers a perfect tetrahedral structure [21]. The highest-occupied molecular orbital and the lowest unoccupied molecular orbital (HOMO-LUMO) gap of Au_{10}^{2+} and its sister Au_{20} are 3.88 and 1.77 eV, respectively, which surpass the value 1.65 eV of the famous C_{60} fullerene [22]. Exceptional stability reported for Au_{10}^{2+} and Au_{20} clusters can be attributed to their magic numbers of 8 and 20 valence electrons, forming a fulfilled electronic shell $1S^2 1P^6$ and $1S^2 1P^6 2S^2 1D^{10}$, respectively. This coincidence of both high-symmetry tetrahedron and closed electronic shell makes Au_{20} and Au_{10}^{2+} magically stable as inert gas atoms.

It is worth to mention that the study of potential superatoms is not limited to the monoatomic species. A considerable amount of experimental and theoretical investigations has been carried out on gold clusters doped with transition metal (M) atoms in order to obtain novel species with the desired structural, magnetic, and chemical properties [23–26]. For instance, Li and coworkers used the laser evaporation technique to produce $M@Au_6$ clusters (M=Ti, V, Cr) in the gas phase and measure their photoelectron spectra using the high-energy laser excimer [27]. The experimental results combined with the density functional theory (DFT) calculations confirm that the magnetic moment of the atomic cluster $M@Au_6$ is tunable by properly selecting the 3d impurity atom. Ehlert's research group discovered that the doping site of the Fe impurity on the $Au_{19}Fe$ and $Au_{18}Fe$ clusters strongly influence the electronic structure and the magnetic moment [28]. Later, Du and coworkers studied the structural evolution of transition metal-doped gold atom cluster $M@Au_{12}$ (M = 3d-5d) by DFT method [29]. While the $Mo/W@Au_{12}$ clusters have icosahedral

cage-like structures, the geometries of the V/Nb/Ta/Tc/Re@Au_{12} clusters tend to form distorted icosahedrons. This structural distortion is explained by the Jahn-Teller effect on the potential field in which electrons move. Recently, the $Au_{19}M$ and Au_9M^{2+} clusters (M=Sc-Ni) have been investigated by Tung and his co-workers [22, 30, 31]. The finding results indicate that the structural growths and electronic properties of $Au_{19}M$ and Au_9M^{2+} clusters are strongly dopant-dependent. However, a general picture comparing the stability patterns and the evolution of structural and electronic properties between $Au_{19}M$ and Au_9M^{2+} clusters has not been done yet. In order to bridge this gap, we present a comparative study on the geometrical, stability, and electronic properties of $Au_{19}M$ and Au_9M^{2+} clusters. Understanding both their similarity and difference will be critical in predicting and designing the superatoms with desirable uses before they are synthesized and used in applications.

2. Computational method

The search for the global minimum geometrics and electronic structures of Au_9M^{2+} and $Au_{19}M$ (M = Sc, Ti, V, Cr, Mn, Fe, Co, and Ni) clusters has been independently re-produced using the density functional theory (DFT) calculations implemented in the Gaussian 09 package [32,33]. For all calculations, predicting geometric structures was pre-optimized using the BP86 functional in conjunction with cc-pVDZ-pp and cc-pVDZ for Au and M atoms, respectively. Details about the calculation setup can be found in Refs. [30,31]. To ensure the robustness of our search method, the isomers with relative energies of less than 2.0 eV (instead of 1.5 eV in previous studies) were selected for accurate single point calculations energies at the same functionality, but combining with a larger basis set, cc-pVTZ-pp for Au atoms and cc-pVTZ for M atoms. This value requires a huge amount of calculations and much more time consuming. The optimization calculations were followed by frequency calculations in order to find the cluster's minimal structures. The electronic configurations of ground-state clusters Au_9M^{2+} and $Au_{19}M$ were explored by using density of state (DOS) and molecular orbitals (MOs). The total/local magnetic moments (TMMs/LMMs) were defined as the difference between the numbers of spin-up and spin-down electrons occupying the molecular/atomic orbitals of the cluster/atom.

3. Results and discussions

3.1. The growth of geometrical structures and spin multiplicities

To investigate the effect of 3d transition metal atoms dopant on pure gold metal clusters Au_{10}^{2+} and Au_{20}, we use an optimization process to determine the clusters' lowest lying structure and electronic configuration. Our first idea came from the pyramid structure of the Au_{10}^{2+} cluster, which resembles that of Au_{20} [20, 34]. The 3d transition metal atoms (M = Sc-Ni) have been substituted by an Au atom in the tetrahedral structures of Au_{10}^{2+} and Au_{20} clusters at different possible positions as the input structures for optimization calculations. The structural evolution of the ground-state Au_9M^{2+} and $Au_{19}M$ (M = Sc, Ti, V, Cr, Mn, Fe, Co, and Ni) clusters is illustrated in Fig. 1. Since our calculations reproduced well the results reported elsewhere, other low-lying isomers of Au_9M^{2+} and $Au_{19}M$ clusters and their relative energies can be found in Refs. [22, 30].

In general, the obtained most stable structures are identical with those reported in Refs. [30, 31]. It is found that the structural geometries and spin multiples of Au_{10}^{2+} and Au_{20} clusters change
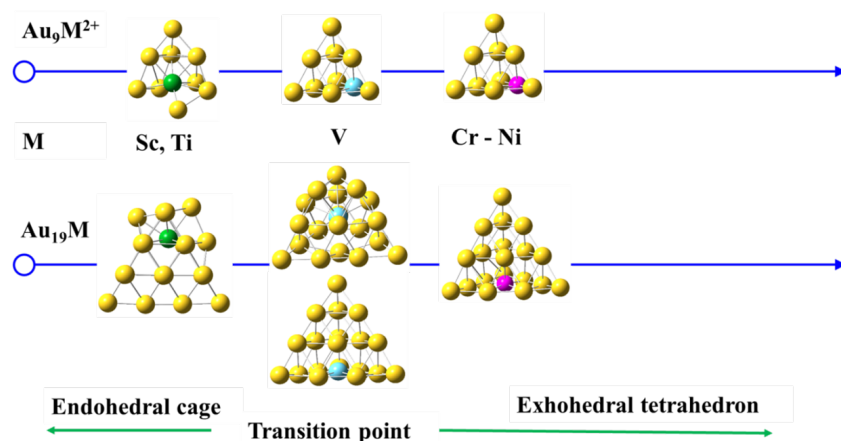
Fig. 1. Structural evolution of the ground-state Au_9M^{2+} and $Au_{19}M$ (M = Sc, Ti, V, Cr, Mn, Fe, Co, and Ni) clusters.

significantly with a M being a first-row 3d transition metal atom. As shown in Fig. 1, the ground-state growth mechanisms on the structures of both Au_9M^{2+} and $Au_{19}M$ clusters are very similar. Their growth mechanism can be separated into two main areas: i) for M = Sc and Ti, the lowest-lying structures of Au_9Sc^{2+}/ $Au_{19}Sc$ and Au_9Ti^{2+}/$Au_{19}Ti$ clusters consistently prefer a cage-like structure with singlet and doublet spin states, respectively. The Sc/Ti dopant atoms occupied the high-coordination position, maximizing the number of (higher in energy [31]) heterobonds with gold atoms; and ii) for heavier dopant atoms (M = Cr-Ni), the ground state structures of Au_9M^{2+} and $Au_{19}M$ clusters favor the slightly distorted tetrahedral of the Au_{10}^{2+} and Au_{20} clusters. In addition, there is a gradual decrease in spin multiplicities from a sextet to a doublet for both species when the dopant atom changes from Cr to Ni. Nevertheless, while the M dopant atoms in Au_9M^{2+} clusters are located on the edge site of the pyramid structure, it is isomorphously substituted for a gold atom at the surface center in the $Au_{19}M$ clusters. This behavior can be understood by the preference of having a maximum number of M-Au bonds for each cluster. Substituting a V for an Au atom on the Au_{10}^{2+}/Au_{20} cluster's tetrahedral structures can be assigned as a transition point transformation from a cage-like structure to a pyramid structure. Although the V dopant seems to be the important ingredient for the structural transformation in both species, it is remarkable that the transformation appears stronger in $Au_{19}V$ compared with Au_9V^{2+}. In particular, the ground-state of the Au_9V^{2+} cluster obviously prefers the form of a pyramid, while the lowest-lying structures of $Au_{19}V$ are the competition between the cage-like structure and the pyramid structure. It is reasonable because with a higher number of gold atoms, the cage-like endohedral $Au_{19}V$ will have more Au-V bonds compared with the highly-symmetric tetrahedral one and consequently slightly more stable.

It is worth considering that, with heavily doped atoms (Cr-Ni), the $Au_{19}M$ cluster can be considered as a combination of its planar Au_{10}^{2-} at the bottom and the tetrahedral sister Au_9M^{2+}. Note that a similar tendency has been observed for the structural evolution of the pyramidal Au_{38} clusters [35]. The lowest-lying structure of Au_{38} is a combination of the well-known 3D pyramidal Au_{20} structure [21,34] and two 2D triangular Au10 [36,37] fragments attached to the 3D pyramidal
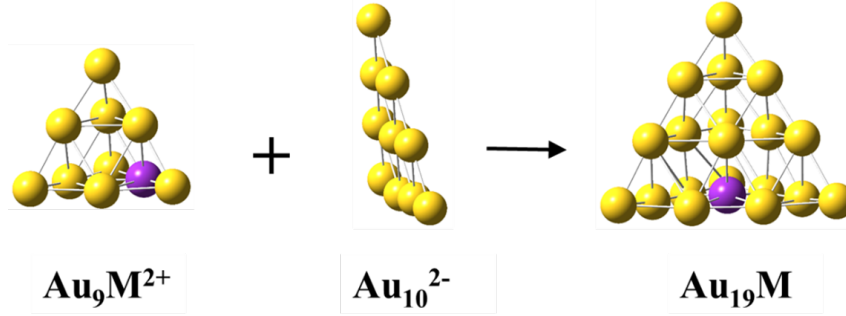
Fig. 2. The smallest pyramid Au_9M^{2+} can be used to construct the larger pyramidal-like gold species like $Au_{19}M$ (M = Cr, Mn, Fe, Co, and Ni) clusters.

Au_{20}. In other words, the Au_{20} pyramid is an important intermediary in the growth mechanism of large-size Au clusters. Ren and his co-workers also illustrated that even bigger clusters could be created by combining the golden Au_{20} clusters together [38]. With this image in mind, it is suggested that the smallest pyramid of Au_{10}^{2+} cluster and its doped species can be used to construct the larger pyramidal-like gold clusters and their doped counterparts beyond Au_{20} and Au_{38} (Fig. 2).

3.2. Stabilities

In order to compare the thermodynamic stability of the Au_9M^{2+} and $Au_{19}M$ clusters, their average binding energies per atom (BE in eV) are re-calculated and compared with those reported in Refs. [30,31]. The BE of a given cluster is a measure of its thermodynamic stability, which is defined as the difference between the energy sum of all the free atoms constituting the cluster and the total energy of the cluster using the following Equations 1 and 2:

$$E_b(Au_{n-1}M^{2+}) = \frac{1}{n}[(n-3)E(Au) + 2E(Au^+) + E(TM) - E(Au_{n-1}M^{2+})] \qquad (1)$$

$$E_b(Au_{n-1}M) = \frac{1}{n}[(n-1)E(Au) + E(TM) - E(Au_{n-1}M)] \qquad (2)$$

where $E(Au)$, $E(Au^+)$, $E(TM)$, $E(Au_{n-1}M^{2+})$, $E(Au_n)$, and $E(Au_{n-1}M)$ are the total energies of the most stable atoms and clusters, respectively. The calculated BE for Au_9M^{2+}, $Au_{19}M$ clusters and AuM dimer are normalized with Au_{10}^{2+}, Au_{20}, and Au_2, respectively, as displayed in Fig. 3. The BE values of the $Au_9M^{2+}/Au_{19}M$ clusters are generally higher than those of pure Au_{10}^{2+}/Au_{20} clusters, especially in the cases of Sc and Ti doped species, suggesting higher relative stabilities of doped clusters. A similar pattern was seen in $Ge_{16}M$ cluster (M = Sc-Ni), where the computed atomic average binding energy of the most stable of $Ge_{16}M$ is typically higher than that of the Ge_{17} cluster [39]. The striking stability enhancement of Sc and Ti doped species can be attributed to the difference in binding energies between Au-M and Au_2 dimers. As shown in Fig. 3, the BEs of Au-Sc and Au-Ti are noticeably stronger than that of Au-Au, while this difference with heavier dopants is less significant. This picture is consistent with the results for Au_5M (M = Sc – Ni) clusters [40], in which the BEs of Au_5Sc and Au_5Ti are also significantly higher than those of Au_6. Our calculation results prove that doping of the first-row transition metal M in general
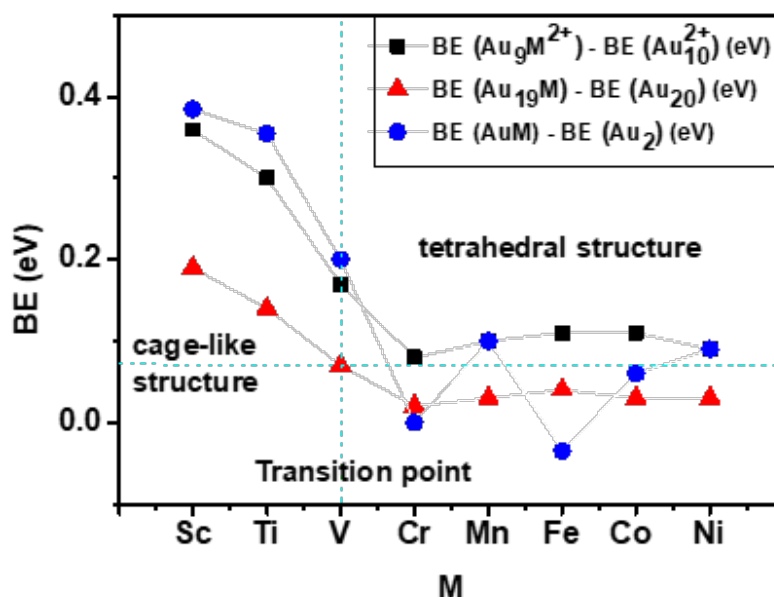
Fig. 3. Binding energy per atom (BE in eV) of Au_9M^{2+}, $Au_{19}M$, and AuM dimers normalized with those of Au_{10}^{2+}, Au_{20}, and Au_2, respectively.

stabilizes the cluster in terms of binding energies compared to their pure counterparts Au_{10}^{2+} and Au_{20}.

It should be noted that the evolution of normalized BE values are quite similar in both Au_9M^{2+} and $Au_{19}M$ as M goes from Sc to Ni with a transition at M = V. However, the normalized BE values of Au_9M^{2+} are higher than those of $Au_{19}\neg M$, especially for M = Sc and Ti. This can be qualitatively explained by the ratio between the number of Au-M bonds and that of Au-Au bonds in each cluster. Since the number of gold atoms in $Au_{19}M$ is much more than in Au_9M^{2+}, the ratio between Au-M bonds and Au-Au bonds in $Au_{19}M$ clusters is smaller than that in Au_9M^{2+}. That gives a reason why the BE values of $Au_{19}M$ are lower than those of Au_9M^{2+}. And since the BEs of cage-like $Au_{19}Sc/Au_{19}Ti$ is not much different from those of tetrahedral $Au_{19}M$ (M = Cr-Ni), it makes the competition between the cage-like structure and the tetrahedral structure more energetically competitive than Au_9M^{2+} species. This result supports the geometric features discussed in the previous section.

Inheriting from the BE of Au-M dimers, the BE evolution of Au_9M^{2+} and $Au_{19}M$ clusters is also divided into two different regimes: i) For the lighter dopants like Sc, Ti, and V, the BEs of Au_9M^{2+} and $Au_{19}M$ are obviously higher, while those with Cr – Ni dopants are lower. The BE values of Au_9M^{2+} and $Au_{19}M$ (M = Cr-Ni) clusters are similar to those of the pure counterparts. It makes Sc/Ti/V impurity favorable in highly-coordinated positions and thus enhances the stability of the doped $Au_{19}M$ and Au_9M^{2+} clusters. ii) At the same time, as shown in Fig. 3, AuM dimers with M = Cr, Mn, Fe, Co, and Ni show an opposite trend, in which their bond strength is somewhat equal to that of an Au_2 dimer. This is why the ground state structures of Au_9M^{2+} and $Au_{19}M$ (M = Cr-Ni) tend to copy those of Au_{10}^{2+} and Au_{20}.

3.3. Electronic properties

In the previous independent work, the spin states of Au_9M^{2+} and $Au_{19}M$ (M = Sc, Ti, Vi, Cr, Mn, Fe, Co, and Ni) clusters have been well explained by the phenomenological shell [22, 30, 31] in which the partial/total outermost valence electrons of M atoms and $6s^1$ valence electrons of Au atoms are assumed to freely delocalize and jointly form a molecular shell of the cluster. The localized electrons remaining on the dopant respond to the cluster magnetic moment [41]. The localized 3d electrons and spin configurations (2S+1) of Au_9M^{2+} and Au9M clusters are shown in Fig. 4. The obtained results are in a good agreement with previous ones [30, 31]. The evolution of spin magnetic moments of Au_9M^{2+} and $Au_{19}M$ (M = Sc-Ni) clusters are identical, varying systematically between 0 μB and 5 μB and depending on the localization of unpaired 3d valence electrons. The largest spin magnetic moment 5 μB is found for Cr doped species Au_9Cr^{2+} and $Au_{19}Cr$. In the previous reports, Au_9Cr^{2+} and $Au_{19}Cr$ have been considered as two stable magnetic superatoms [22, 30, 31]. Therefore, the aim of this section is to discuss the underlying physics and to compare the magnetic behavior of Au_9Cr^{2+} and $Au_{19}Cr$ systems, and possibly generalize a mechanism to predict the magnetic behavior in similar quantum systems.
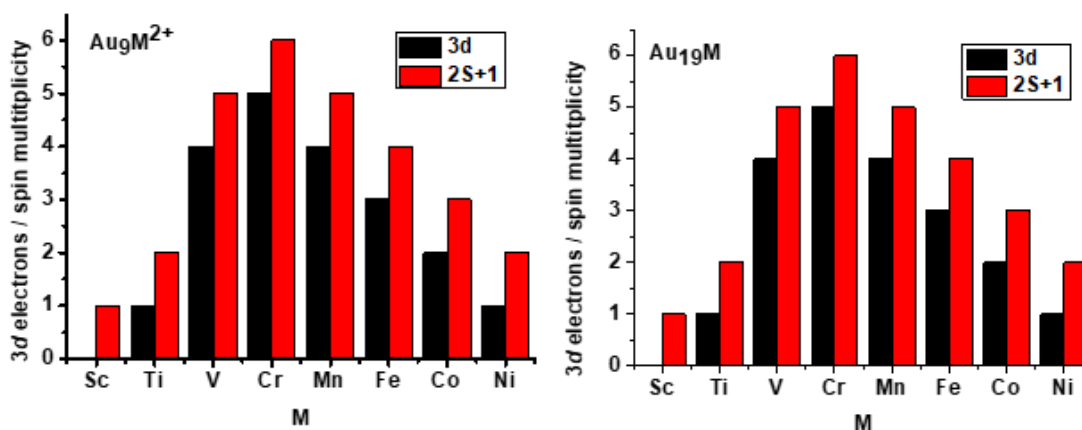
Fig. 4. The localized 3d electrons and spin multiplicity of Au_9M^{2+} and $Au_{19}M$ (M = Sc, Ti, V, Cr, Mn, Fe and Ni), respectively.

Doping a Cr atom into Au_{10}^{2+} and Au_{20} clusters results in the formation of an electronic shell structure of delocalized electrons and a magnetic shell of localized/unpaired ones. The shapes of the relevant molecular orbitals (MOs) and their energy levels for Au_9Cr^{2+} and $Au_{19}Cr$, as illustrated in Fig. 5, reveal the great similarity between their densities of states (DOS) and hence demonstrate the similarity in their electronic structures as well as their thermochemical stability. It can be seen from Fig. 5, the MOs of Au_9Cr^{2+} and $Au_{19}Cr$ clusters obviously separate into intense bands. The energy bands of Au_9Cr^{2+} lie at -19 eV (1S), between -18 eV and -15 eV (1P), at 14 eV (2S), and between -13 eV and -12 eV (HOMO). Those of $Au_{19}Cr$ are correspondingly at -12 eV (1S), between -11 eV and -10 eV (1P), at -9 eV (2S), between -8 eV and -6 eV (1D), and at -5.5 eV (HOMO). In the lower band, while the MOs of Au_9Cr^{2+} have four filled orbitals (one 1S, first two 1P and one 2S orbitals), $Au_{19}M$ contains ten filled orbitals (one 1S, three 1P, one 2S, and five 1D orbitals). For both clusters, the lowest-lying MOs include 1S subshell, which is mainly composed

of s-AO of Au. The second-lying MOs of Au_9Cr^{2+} and $Au_{19}Cr$ clusters correspond to two and three p-type orbitals of the 1P subshells, respectively. Unlike the electronic structure of $Au_{19}Cr$, the electron configuration of tetrahedral Au_9Cr^{2+} undergo an 1P splitting. The phenomenon can be plausibly explained by the fact that the oblate distortion may excite a compression along the z axis, leading to an upward shift of the 1Pz orbitals relative to the 2S one. That is considered the main cause of the formation of the 8-electron shell closure $1S^21P^42S^2$ for Au_9Cr^{2+} cluster. The MOs of 2S subshell of Au_9Cr^{2+} are located at an energy level of -14 eV, whereas the one of $Au_{19}Cr$ lie at about -7 eV. The highest bands of both Au_9Cr^{2+} and $Au_{19}Cr$ consist of five half-filled localized Cr-dopant d orbitals, which is the origin of the doped cluster's magnetic moment. It turns out that the electronic configuration of the Au_9Cr^{2+} and $Au_{19}Cr$ cluster basically satisfies the electronic shell model of $1S^21P^42S^23d^5_\uparrow$ and $1S^21P^62S^21D^{10}3d^5_\uparrow$ with a corresponding magnetic moment of 5 μB, respectively.
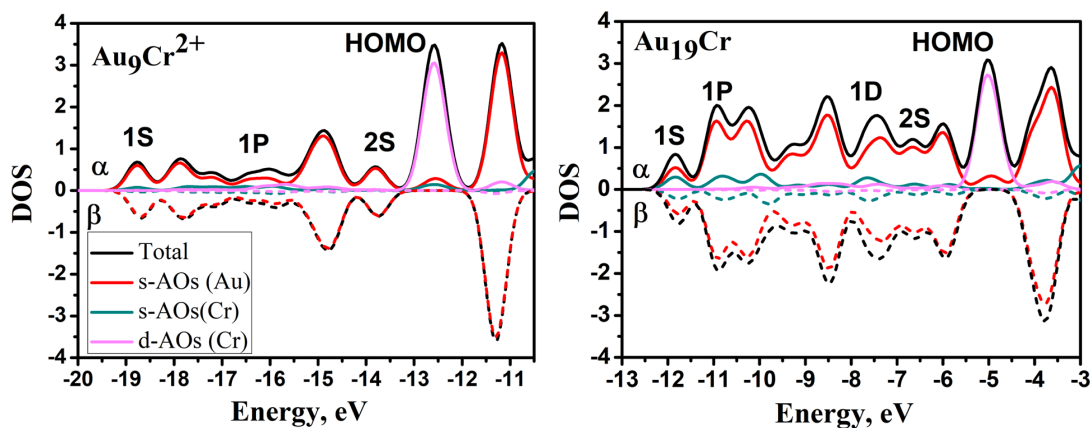
Fig. 5. Total (DOS) and partial (pDOS) density of state of the most stable Au_9Cr^{2+} and $Au_{19}Cr^{2+}$ clusters.

4. Conclusion

The golden pyramid Au_{10}^{2+} and Au_{20} clusters doped with 3d transition metal atoms (Sc-Ni) were examined by using density functional theory. The similarities and differences between their structural, stability, and electronic properties were discussed and compared. It is found that the structural evolution and stable patterns of Au_9M^{2+} cluster resemble that of $Au_{19}M$ in general. From Sc to Ni, the V dopant is the transition point for the structural transformation in both species. The transformation appears stronger in $Au_{19}V$ compared with Au_9V^{2+}. Substituting an Au atom by a transition metal atom (M = Sc-Ni) in general can enhance the stability of clusters. Both Au_9Cr^{2+} and $Au_{19}Cr$ have similarities in the electronic structures and are potential magnetic superatoms. $Au_{19}M$ (M = Cr- Ni) cluster can be considered as a combination of a triangular Au_{10}^{2-} and its smallest copy Au_9M^{2+}. We believe that our findings can serve as a premise to understand and predict the formation of larger pyramidal-like gold species and their stable superatoms in the future.

Acknowledgment

Conflict of interest

The authors have no conflict of interest to declare.

References

[1] Y. Gao, N. Shao, Y. Pei, Z. Chen and X. C. Zeng, *Catalytic activities of subnanometer gold clusters (Au16–Au$_{18}$, Au$_{20}$, and Au$_2$7–Au35) for CO oxidation*, ACS Nano **5** (2011) 7818.

[2] Y. Sun, X. Liu, K. Xiao, Y. Zhu, and M. Chen, *Active-site tailoring of gold cluster catalysts for electrochemical CO$_2$ reduction*, ACS Catalysis **11** (2021) 11551.

[3] M.-W. Chang, L. Zhang, M. Davids, I. A. W. Filot and E. J. M. Hensen, *Dynamics of gold clusters on ceria during CO oxidation*, J. Catalysis **392** (2020) 39.

[4] S. Zhu, X. Wang, Y. Cong and L. Li, *Regulating the optical properties of gold nanoclusters for biological applications*, ACS Omega **5**(36) (2020) 22702.

[5] P. Pyykko, *Theoretical chemistry of gold. III*, Chem. Soc. Rev. **37** (2008) 1967.

[6] R. Olson, S. Varganov, M. Gordon, H. Metiu, S. Chretien, P. Piecuch, K. Kowalski, S. Kucharski, M. Musial, *Where does the planar-to-nonplanar turnover occur in small gold clusters?*, J. Am. Chem. Soc. **127** (2005) 1049.

[7] M. Gruber, G. Heimel, L. Romaner, J. L. Bredas, E. Zojer, *First-principles study of the geometric and electronic structure of Au13 clusters: Importance of the prism motif*, Phys. Rev. B **77** (2008) 165411.

[8] P. Gruene, D. M. Rayner, B. Redlich, A. F. G. van der Meer, J. T. Lyon, G. Meijer, A. Fielicke, *Structures of neutral Au$_7$, Au$_{19}$ and Au$_{20}$ clusters in the gas phase*, Science **321** (2008) 674.

[9] S. Bulusu, X. Zeng, *Structures and relative stability of neutral gold clusters: Au$_n$ (n=15-19)*, J. Chem. Phys. **125** (2006) 154303.

[10] W. Fa, J. Dong, *Possible ground-state structure of Au$_2$6: A highly symmetric tubelike cage*, J. Chem. Phys. **124** (2006) 114310.

[11] X. Xing, B. Yoon, U. Landman and J.H. Parks, *Structural evolution of Au nanoclusters: From planar to cage to tubular motifs*, Phys. Rev. B **74** (2006) 165423.

[12] M. Johansson, D. Sundholm and J. Vaara, *Au$_{32}$: A 24-carat golden fullerene*, Angew. Chem. Int. Ed. **43** (2004) 2678.

[13] M. Walter, J. Akola, O. Lopez-Acevedo, P. Jadzinsky, G. Calero, C. Ackerson, R. Whetten, H. Gronbeck, H. Hakkinen, *A unified view of ligand-protected gold clusters as superatom complexes*, Proc. Natl. Acad. Sci. U. S. A. **105** (2008) 9157.

[14] Y. Gao, N. Shao, Y. Pei, Z. Chen, X. Zeng, *Catalytic activities of subnanometer gold clusters (Au16-Au$_{18}$, Au$_{20}$ and Au$_2$7-Au35) for CO oxidation*, ACS Nano **5** (2011) 7818

[15] A. Sanchez, S. Abbet, U. Heiz, W.-D. Schneider, H. Ha1kkinen, R. N. Barnett and Uzi Landman, *When gold is not noble: nanoscale gold catalysts*, J. Phys. Chem. A **103** (1999) 9573

[16] F. Remacle and E. Kryachko, *Novel features in 2D and 3D neutral, cationic, and anionic gold clusters Au$_{5 \le n \le 8}^Z$ (Z = 0, ±)*, arXiv:physics/0412077 (2005).

[17] L. Ferrighi, B. Hammer and G. K. Madsen, *2D – 3D transition for cationic and anionic gold clusters: a kinetic energy density functional study*, J. Am. Chem. Soc. **131** (2009) 10605.

[18] M. P. Johansson, A. Lechtken, D. Schooss, M. M. Kappes and F. Furche, *2D-3D transition of gold cluster anions resolved*, Phys. Rev. A **77** (2008) 053202.

[19] P. V. Nhat, N. T. Si, N. T. N. Hang and M. T. Nguyen, *The lowest-energy structure of the gold cluster Au 10: planar vs. nonplanar?*, Phys. Chem. Chem. Phys. **24** (2022) 42.

[20] P. M. Petrar, M. B. Sárosi and R. B. King, *Au$_{10}^{2+}$: a tetrahedral cluster exhibiting spherical aromaticity*, J. Phys. Chem. Lett. **3** (2012) 3335

[21] E. Kryachko and F. Remacle, The magic gold cluster Au$_{20}$, Int. J. Quantum Chem. **107** (2007) 2922.

[22] N. T. Lan et al., *DFT investigation of Au_9M^{2+} nanoclusters (M= Sc-Ni): The magnetic superatomic behavior of Au_9Cr^{2+}*, Chem. Phys. Lett. **793** (2022) 139451.

[23] E. Janssens, *Electronic and geometric structure of transition metal doped silver and gold clusters*, PhD Thesis, Katholieke Universiteit Leuven (2004).

[24] A. Ghosh, O. F. Mohammed and O. M. Bakr, *Atomic-level doping of metal clusters*, Acc. Chem. Res. **51** (2018) 3094

[25] L. Pečinka, E. M. Peña-Méndez, J. E. Conde-González and J. Havel, *Laser ablation synthesis of metal-doped gold clusters from composites of gold nanoparticles with metal organic frameworks*, Sci. Rep. **11** (2021) 4656.

[26] S. Neukermans, E. Janssens, H. Tanaka, R. Silverans and P. Lievens, *Element-and size-dependent electron delocalization in Au_NX^+ clusters (X= Sc, Ti, V, Cr, Mn, Fe, Co, Ni)*, Phys. Rev. Lett. **90** (2003) 033401.

[27] X. Li, B. Kiran, L. F. Cui and L. S. Wang, *Magnetic properties in transition-metal-doped gold clusters: $M@Au_6$ (M = Ti, V, Cr), (in eng)*, Phys. Rev. Lett. **95** (2005) 253401.

[28] C. Ehlert and I. P. Hamilton, *Iron doped gold cluster nanomagnets: ab initio determination of barriers for demagnetization*, Nanoscale Adv. **1** (2019) 1553.

[29] Q. Du *et al.*, *Structure evolution of transition metal-doped gold clusters $M@Au_{12}$ (M = 3d-5d): across the periodic table*, J. Phys. Chem. C **124**(13) (2020) 7449.

[30] N. M. Tam, N. T. Mai, H. T. Pham, N. T. Cuong and N. T. Tung, *Ultimate Manipulation of magnetic moments in the golden tetrahedron Au_{20} with a substitutional 3d impurity*, J. Phys. Chem. C **122** (2018) 16256.

[31] N. M. Tam, N. T. Cuong, H. T. Pham and N. T. Tung, *$Au_{19}M$ (M=Cr, Mn and Fe) as magnetic copies of the golden pyramid*, Sci. Rep. **7** (2017) 16086.

[32] M. Frisch *et al.*, Gaussian 09 (Revision A02), Gaussian Inc. Wallingford CT, (2009).

[33] P. Hohenberg and W. Kohn, *Inhomogeneous electron gas*, Phys. Rev. **136**(3B) (1964) B864.

[34] J. Li, X. Li, H.-J. Zhai and L.-S. Wang, *Au_{20}: a tetrahedral cluster*, Science **299** (5608) (2003) pp. 864-867.

[35] N. Shao, W. Huang, L.-S. Wang, Q. Wu and Z. Cheng, *Structural evolution of medium-sized gold clusters Au_n^- (n = 36, 37, 38): appearance of bulk-like face centered cubic fragment*, J. Phys. Chem. C **118** (2014) 6887.

[36] H. Hakkinen, B. Yoon, U. Landman, X. Li, H.-J. Zhai and L.-S. Wang, *On the electronic and atomic structures of small Au_{N^-} (N = 4-14) clusters: a photoelectron spectroscopy and density-functional study*, J. Phys. Chem. A **107** (2003) 6168.

[37] W. Huang and L.-S. Wang, *Au_{10}^-: isomerism and structure-dependent O_2 reactivity*, Phys. Chem.Chem. Phys. **11**(15) (2009) pp. 2663.

[38] L. Ren and L. Cheng, *Structural prediction of $(Au_{20})_N$ (N = 2–40) clusters and their building-up principle*, Comput. Theor. Chem. **984** (2012) 142.

[39] H. T. Nguyen, N. T. Cuong, N. T. Lan, N. T. Tung, M. T. Nguyen and N. M. Tam, *First-row transition metal doped germanium clusters $Ge_{16}M$: some remarkable superhalogens*, RSC advances **12**(21) (2022) 13487.

[40] Z. Ben-Xia, D. Dong, W. Ling and Y. Ji-Xian, *Density functional study on the structural, electronic and magnetic properties of 3d transition-metal-doped Au_5 clusters*, J. Phys. Chem. A **118** (2014) 4005.

[41] J. Reveles *et al.*, *Designer magnetic superatoms*, Nature Chem. **1** (2009) 310.